Numerical Investigation of Negative Temperature Coefficient Effects on Sooting Characteristics in a Laminar Co-flow Diffusion Flame

Han Wu, Zhen Hu, Xu Dong, Saifei Zhang,* Zhikun Cao, and Sheng-lun Lin

ACCESS | Metrics & More | Article Recommendations

ABSTRACT: It is a common sense that diesel engines produce worse soot emission than gasoline engines, even though gasoline direct injection also brings about terrible sooting tendency. However, reports showed that diesel emits less soot than gasoline in laminar diffusion flames, which implies that soot emission is a combined effect of multiple factors, such as the combustion mode, physical properties of the fuel, and also fuel chemistry. This work, thus, conducted numerical calculations in laminar co-flow diffusion flames of fuels with different negative temperature coefficient (NTC) behaviors in an order of *n*-heptane > iso-octane > toluene to solely evaluate the chemical effect, especially the role of low-temperature combustion on soot formation. 2-Dimensional simulations were carried out to obtain the soot distributions, and 0-dimensional simulations were performed to analyze the chemical kinetics of polycyclic aromatic hydrocarbon (PAH) formation and low-temperature reaction sensitivities. The grids of the 2-D model converged at $80(r) \times 196(z)$, and the boundary conditions of both models were set to eliminate the influence of physical factors as much as possible. The results showed that there were three main reactions associated to the formation of aromatic hydrocarbons A1 at the first-stage combustion in the *n*-heptane flame and the iso-octane flame, in which the reaction of $C_7H_{15} + O_2 = C_7H_{15}O_2$ enhances the NTC behavior. The first two reaction pathways generated larger molecular hydrocarbons and were unfavorable by A_1 formation and therefore inhabit the PAH formation, and 49.8% of C_7H_{16} reacted through the large molecular pathways, while the percentage for C_8H_{18}, with weaker NTC behavior, was only 37%. Toluene with even weaker NTC behavior showed no low-temperature oxidation. Therefore, in a more general case, fuels with stronger NTC behavior smoke less, and this conclusion could be promising potential to reduce soot emission in future.
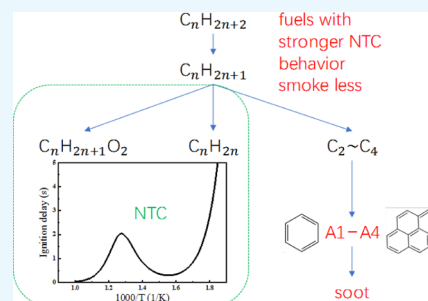
1. INTRODUCTION

Soot originates from the heterogeneous combustion of hydrocarbon fuels, which is extremely harmful to human health and the environment.[1−4] In the transportation sector, not only heavy-duty diesel engines suffer from their infamous soot emission reputation but also the recent emerging market GDI engines show significantly high soot emission tendency. Within this scenario, increasingly strict emission regulations were imposed all over the world and soot emission control has become a public priority.

Many researchers have conducted experimental observations on the sooting tendency among actual engines fueled with diesel, gasoline, and their blends.[5−7] It is agreed that the soot emissions from port fuel injection (PFI) gasoline engines is quite low[8] due to the comparatively high volatility that is suitable for the premix combustion mode. On the contrary, diesel engines incline to exhaust more soot emission since diesel with a lower auto-ignition temperature and low volatility is usually used in the compression−ignition (CI) engines and bears non-premix combustion.[9] Moreover, the optical results from Zheng et al.[10] proved that the addition of gasoline into diesel would reduce soot production as a result of an increased liftoff flame length and better air−fuel mixing. However, these observations do not necessarily imply that gasoline with a lighter average molecular weight emits less soot than diesel. In fact, some direct-injection gasoline engines emit just as many soot particles as unfiltered diesel cars did in the past.[11] In addition, in a fundamental flame research conducted by Liu et al.[12] that compared the sooting tendency of gasoline/diesel blend flames on a liquid burner with the diffuse 2D-LOSA technology, the 2-dimensional soot volume fraction value decreases as the proportion of diesel in the gasoline/diesel mixture increases, which indicates that diesel is less likely to produce soot than gasoline in a laminar diffusion flame. Therefore, it can be speculated that the sooting characteristics in an actual engine are influenced by the combined effects of multiple factors, such as the combustion mode, physical properties of the fuel, and also fuel chemistry.
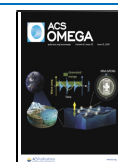
As is known, the soot generation tendency of different fuels varies largely from fuel to fuel due to different molecular structures,[13−16] so the fuel chemistry plays a critical role in the soot formation. However, it is not easy to evaluate a single effect through an internal combustion engine or a constant volume chamber experiment since the combustion processes inside them are comprehensive physical−chemical combined processes. Thus, different kinds of fundamental flames have been wildly used to separate the chemical process out of other factors, and many academic fruits have been achieved on the soot formation.[17−19]

Polycyclic aromatic hydrocarbons (PAHs) are the most widely accepted precursors in the nucleation stage of soot particles.[20,21] There are many kinds of PAHs, including benzene (A1), naphthalene (A2), phenanthrene (A3), pyrene (A4), and other larger aromatic hydrocarbons. Different fuels own different molecular structures, which determine the PAH formation ability, and thus the respective sooting tendency. Oxygenated fuels, such as methanol, ethanol, butanol, and so forth, form less PAHs and soot due to the oxidation effect.[22−24] Aromatic hydrocarbon fuels, such as toluene, n-propyl benzene, and so forth, are easy to form PAHs and promote the soot nucleation.[25−28] Mechanisms for the formation of soot have also been extensively studied since the 1990s,[29−32] among which the hydrogen abstraction carbon addition (HACA) theory is widely accepted for the growth process from A1 to high-ring PAHs.[33,34] The mechanism argued that the first step in the soot formation process is the generation of the soot precursor, especially the generation of the first benzene ring (A1) trough $C_4H_4 + C_2H_2 = C_6H_6$ and $2C_3H_3 = C_6H_6$,[35] and the speed of this step determines the subsequent soot generation. After precursor formation, the aromatic ring grows further following the steps precursor formation, particle inception, surface growth and agglomeration, and particle oxidation. High-ring PAHs condense to form soot. Zhang et al.[36] conducted simulation studies in the two-dimensional laminar CH_4/air diffusion flame mixed with vaporized gasoline surrogates, and the addition of the PAH coagulation mechanism can make the results more accurate with the experimental data.

Liu et al.[15] in our research group investigated the sooting characteristics of gasoline/diesel blends on a laminar co-flow diffusion flame. They found that when the fuel with stronger low-temperature reaction is combusted, the cold flame zone increased and the amount of soot is reduced. The speculation is that the enhancement of cold flame combustion, due to its stronger negative temperature coefficient (NTC) behavior of the diesel fuel, is a cause of soot reduction. NTC behavior is a phenomenon that occurs during low-temperature to high-temperature reaction for certain fuels.[37] Its effects on auto-ignition have been extensively understood and researched.[38] However, its effects on soot emissions have rarely been researched.

By reason of the foregoing, this work focuses on revealing the chemical effects of the NTC behavior on the soot characteristics precisely. Since the diffusion flame test of the liquid fuel with a high-boiling point is highly sensitive to the supply fluctuation,[12] experimental studies are hard to carry out. This study therefore conducted numerical calculations of three different fuels with different NTC behaviors in the order of n-heptane > iso-octane > toluene. 2-D and a 0-D diffusion flame models were set up and the boundary conditions are set to eliminate the influence of physical factors as much as possible

so that the study can focus on the influence of low-temperature chemical reaction and NTC behavior.

2. NUMERICAL METHODS

2.1. Chemical Mechanism. The chemical mechanism used in the simulations is a simplified toluene reference fuel (TRF, n-heptane/isooctane/toluene) mechanism developed by An et al.,[9] which includes 85 species and 232 reactions. This mechanism was validated against test results of ignition delays, premixed laminar flame speeds, profiles of key species, and PAH concentrations from the shock tube, adiabatic flat flame burner, and GDI engine data, respectively, and showed reliable and promising performances in the reproduction of auto-ignition and flame propagation characteristics and PAH predictions at both low and high pressures. Furthermore, its reduced size saves calculation time when coupled in 2-D and 3-D CFD simulations. In this work, the low-temperature region is defined as the flame temperature under 1000 K, and the high-temperature reaction starts from 1000 K. With this scenario, the mechanism contains low-temperature reactions as shown in Table 1 and is able to simulate the NTC behavior

Table 1. Low-Temperature Reactions in An's Mechanism

R2	$C_7H_{15} + O_2 = C_7H_{15}O_2$
R3	$C_7H_{15}O_2 = C_7H_{14}OOH$
R4	$C_7H_{14}OOH + O_2 = O_2C_7H_{14}OOH$
R5	$O_2C_7H_{14}OOH \geq C_7KET + OH$
R6	$C_7KET \geq C_5H_{11}CO + CH_2O + OH$
R16	$C_8H_{17} + O_2 = C_8H_{17}O_2$
R17	$C_8H_{17}O_2 = C_8H_{16}OOH$
R18	$C_8H_{16}OOH + O_2 = O_2C_8H_{16}OOH$
R19	$O_2C_8H_{16}OOH \geq C_8KET + OH$
R20	$C_8KET \geq C_6H_{13}CO + CH_2O + OH$

accurately. If the initial boundary temperature is low, the fuel undergoes the low-temperature reactions before entering the high-temperature reaction stage.

2.2. 2-D Simulation of a Laminar Diffusion Flame. The previous experiment work in our group indicated that the cool flame zone in the laminar co-flow diffusion flames varied as the fuel changed, and soot emission reduced as the cool flame zone enlarged.[39] In order to verify the relationship between cool flames, the low-temperature reactions, and the soot formation more intuitively with a theoretical basis, a 2-D Coflame numerical model was established to simulate laminar diffusion flames of n-heptane, iso-octane, and toluene. This model is capable of calculating the temperature field, the concentration field of each component, the volume fraction of soot, the nucleation rate, the number density of soot, and also the dynamic evolution of smoke particles. The simulation domain and boundary conditions were set according to Liu's work.[39] As shown in Figure 1, the calculation domain represents a coaxial laminar diffusion flame. The inner diameter of the fuel outlet is 10.9 mm, the wall thickness of the pipe is 1 mm, and the air outlet is a concentric tube with an inner diameter of 58 mm. The flow rate of fuel vapor is 7 g/h and that of the carrier gas N_2 is 0.3 L/min, so the fuel vapor takes up 11% in the fuel mixture. The oxidant air is composed of 79% nitrogen and 21% oxygen and flows through the outer tube with a rate of 200 L/min. The initial temperature is 523 K.

The diffusion and convection terms in governing equations are discretized using the center difference and upwind
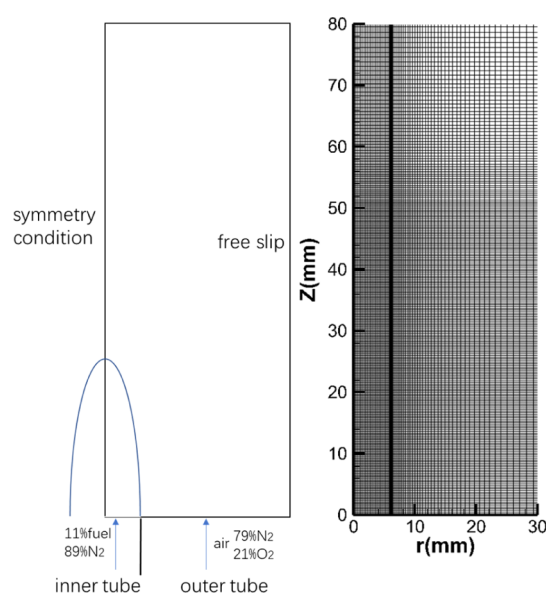
Figure 1. Boundary conditions and the grid in the 2-D simulation.

mm in length, and the outer domain filled with air is meshed to 0.2525 mm × 1.04^n, where n is the nth grid.

The free-slip boundary condition and zero gradient boundary condition are set at the axial and vertical directions. After a sensitivity analysis, the calculation domain is proved to be large enough and the boundary position does not affect the simulation results. To verify the convergence of the grid, more sets of denser grids up to $120(r) \times 320(z)$ are used in the test calculations, and their corresponding results showed little differences from that of the $80(r) \times 196(z)$ grids. Therefore, the $80(r) \times 196(z)$ grids are believed to be good enough for the evaluations of flame characteristics. The convergence precision is set as 10^{-5}.

2.3. 0-D Simulation to Research the Mechanism. Even though the 2-D simulation has merits in visualization, it is deficient in conducting the further chemical analysis since it is still a physical−chemical coupled process. Therefore, a 0-D simulation is carried out to analyze the chemical factors that impact the formation of PAHs and soot. The constant-pressure homogeneous reactor in CHEMKIN 17.0 software was used to simulate the cool flame and low-temperature reaction process of the individual n-heptane and iso-octane flames. Toluene hardly reacts at low temperatures.

When analyzing the relationship between NTC behavior and PAH formation, the n-heptane and iso-octane flames are stoichiometric flames under atmospheric pressure. The initial temperature changes from 500 to 1000 K. When studying soot forming characteristics for rich flames of n-heptane and iso-octane, the pressure is set to be 30/60 atm and the equivalence ratio is set as 1.0/3.0. The initial temperature changes from 700 to 1300 K.

difference schemes, respectively. To speed up the convergence rate, the triangular matrix algorithm (TDMA) is adopted to solve the momentum, energy, and pressure correction equations, and the discrete equations of gas composition, soot mass fraction, and soot density are solved using the full coupling method. In addition, the parallel computation method is used to increase the calculation efficiency. The calculation domain is meshed to an $80(r) \times 196(z)$ grid in the r and z directions, respectively, where $z = 0$ represents the outlet plane of the fuel and air and $r = 0$ represents the symmetrical plane of the diffusion flame. Non-uniform grids are adopted to lower the model error and reduce time consumption; the mesh inside the inner tube is 0.2725 mm in length, the interface between the fuel and air is meshed to 0.1

3. RESULTS AND DISCUSSION

3.1. Phenomenon of NTC Effects on Soot Formation. The simulated 2-D temperature distribution around the root of the n-heptane and iso-octane flames is obtained through the Coflame software, as shown in Figure 2a,b. It is seen that there
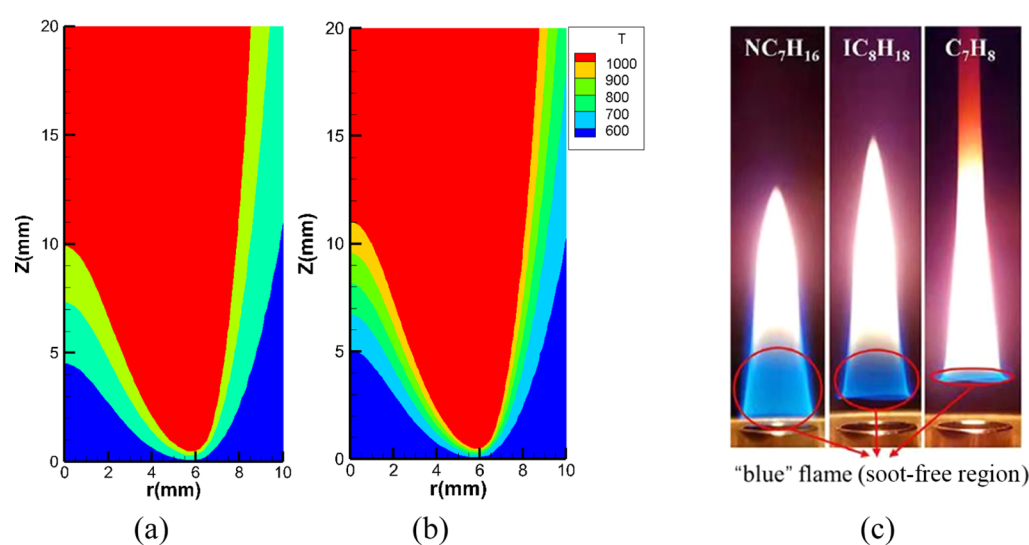

Figure 2. Temperature distributions near the root of in the n-heptane and iso-octane flames and the experiment flame structures of TRF individual fuels.[15] (a) n-Heptane, (b) iso-octane, and (c) experiment flame structure.[15] Image (c) is reprinted with permission from [Liu, F.; Hua, Y.; Wu, H.; Lee, C. Effect of Toluene Addition on the PAH Formation in Laminar Coflow Diffusion Flames of n-Heptane and Iso-octane. *Energy Fuels.* **2018**, 32(6), 7142−7152]. Copyright [2018] [Energy and Fuels.]. Photograph courtesy of "Liu, Fushui and Hua, Yang". Copyright 2018. Permission is not needed since the image is sourced from another ACS journal Energy and Fuels.
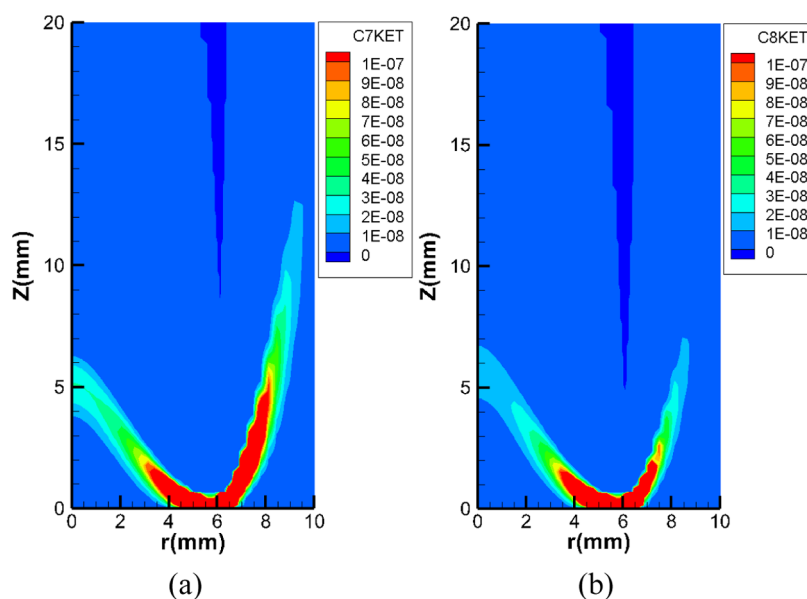
Figure 3. Keto-peroxide C_7KET and C_8KET distributions in the *n*-heptane and iso-octane flames, (a) *n*-heptane flame and (b) iso-octane flame.

is a low-temperature zone ranging from 600 to 1000 K near the burner outlet, colored from blue to yellow surrounding the red high-temperature zone. It is believed that when the region temperature is below 600 K, the ignition temperature is not reached, so there is no flame in this region. When the temperature is above 700 K, the first stage of ignition occurs and the "cold flame" begins to develop. When the temperature goes up to around 1000 K, the second ignition take place and the hot-temperature reactions become intensified and produce a rather "hot flame". Therefore, in this work, the low-temperature region is defined as the flame temperature under 1000 K, and when the flame temperature is above 1000 K, the hot temperature reaction starts. According to the temperature distribution, the flames around the outlet are hollow-cone-shaped with a "cool flame" surrounding the "hot flame" structure.

The simulation is consistent with the previous experiment in our group,[15,39] as shown in Figure 2c. The experiment results show that there are two obvious flame regions in the flames. The bright "yellow" flames at the upper side of the flame are reflections of soot incandescence, which indicate a strong soot accumulation. However, the weak "blue" flames at the bottom indicate that the luminosity is dominated by the chemiluminescence, which implies that these zones are "soot-free". On the other hand, the two distinct regions can be roughly seen as an indication of an obvious two-stage ignition of fuels. The start of the "blue" flame represents the first stage of ignition, where low-temperature oxidation occurs and the "cool flame" takes place, while the start of the "yellow" flame represents the second stage of ignition, where high-temperature oxidation and the "hot flame" dominate. The transition process from low-temperature oxidation to hot-temperature oxidation, where the chemical reaction rate slows down to accumulate OH$^+$ radicals and heat, forms the NTC phenomenon. Therefore, the length of the "blue" flame can be considered as an indicator of the intensity of the NTC tendency of a fuel. That is to say, the stronger the NTC tendency is, the longer gap the two-stage combustion has and the lengthier the "blue" flame becomes, which obtains a boarder "soot-free" zone and contributes to the imaginable soot reduction.

3.2. Key Intermediate Distributions. Keto-peroxides C_7KET and C_8KET are the key intermediates that are produced in the *n*-heptane and iso-octane flames under low-temperature reactions for keto-peroxides are generally temperature-sensitive intermediate products that only exist at the low-temperature region. Figure 3 shows the two keto-hydro-peroxide distributions in their corresponding flame. The C_7KET radicals in the *n*-heptane flame are generated through reaction R5 according to low-temperature reaction shown in Table 1, and it is relatively stable at low temperatures but soon dissociates into $C_5H_{11}CO$, CH_2O, and OH radicals through reaction R6 as the temperatures rise above 800 K. Therefore, C_7KET can indirectly reflect low-temperature reaction intensity.

At HAB (height above burner) = 0, the fuel vapor just emerges from the fuel outlet to meet the oxidant air from the outer tube. The temperature at this time is quite low, and the low-temperature reactions take place at once. The reactions begin to generate the most C_7KET around the outlet interface and make the temperature rise quickly. As the flame height increases, the flame temperature increases too and develops into the high-temperature region rapidly, and the C_7KET radicals vanish dramatically as the flame height increases. At the same time, the oxidant air from the outer tube propagates to the flame center through diffusion, and the low-temperature reactions occur accordingly at the regions far from the outlet interface. It is reasonable that as the flame height increases, the fuel and air inter-diffuse more, so the low-temperature reaction band becomes more spread. Therefore, the C_7KET distribution presents a tick-mark-shaped band.

The distribution of the keto-peroxides C_8KET in the iso-octane flame is similar to that in the *n*-heptane flame. Comparing the two distributions, C_7KET radicals extend further due to the longer transitioning period from low-temperature reaction to high-temperature reaction, that is, the NTC effects. The higher and wider C_7KET region also corresponds to the phenomenon that the "blue" flame region of *n*-heptane is larger than that of iso-octane. Since toluene has little low-temperature oxidation, the corresponding products in

the toluene fuel barely exist. This explains why the "blue" flame in the toluene flame has the minimum size.

The amount of the keto-peroxides of the *n*-heptane and iso-octane flames on the central axis is provided in Figure 4 as a
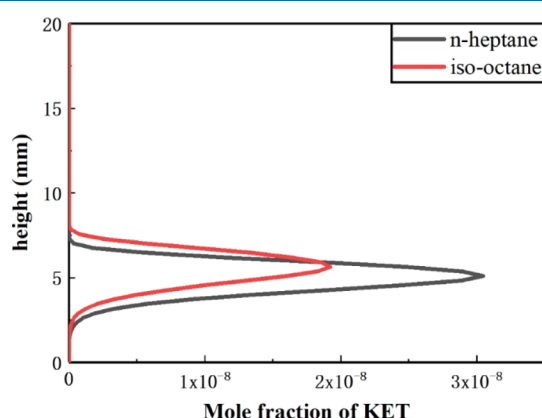

Figure 4. Distributions of keto-peroxides of the *n*-heptane and iso-octane flames on the central axis.

more quantitative piece of evidence. At an HAB of 2 mm, the flame of *n*-heptane started to generate C_7KET, which implies that the air supplied from the outer tube has arrived the central axis. The amount of C_7KET radicals increases rapidly along the central axis from then on and peaks at an HAB of 5 mm. As the low-temperature reaction keeps proceeding, the temperature increases gradually and low-temperature reactions are suppressed after that. Therefore, the mole fraction of C_7KET radicals finally decreases to 0 at an HAB of 7 mm. The keto-peroxide C_8KET distribution shows a similar trend to that of the C_7KET, which offsets a bit higher due to the longer first-stage ignition delay and the higher auto-ignition temperature. This corresponds to the higher liftoff height of the isooctane flame in the experiment shown in Figure 2. The mole fraction of C_8KET peaks at an HAB of 6 mm with a lower quantity, indicating that the low-temperature reaction intensity of the iso-octane flame is weaker along the central axis due to the

faster transition from low-temperature reaction to high-temperature reaction, which is a weaker NTC effect.

When the temperature increases beyond 800 K, the keto-hydroperoxides $C_7H_{14}OOH$ produce aldehydes rather than C_7KET. Aldehydes form immediately at the beginning of the first stage of ignition and disappear dramatically when the second stage of ignition starts. Formaldehyde, CH_2O, is the most abundant of all aldehyde products, so it is often seen as an important index to reflect the evolution process from low-temperature reaction to high-temperature reaction. The electronically excited formaldehyde illuminates a pale "blue" chemiluminescence, which makes the CH_2O radicals a more direct indicator of the "blue" flame and NTC behavior.

The 2-D distributions of CH_2O radicals in the respective *n*-heptane, iso-octane, and toluene flames are shown in Figure 5. The distribution of CH_2O radical in the *n*-heptane flame is wider than that in the iso-octane flame, whereas only a very slight CH_2O radical distribution is seen in the toluene flame due to the barely happened low-temperature reactions. Both *n*-heptane and iso-octane flames generate a large amount of CH_2O in the area around $r = 6$ mm and HAB = 0−2 mm, which correspond to the distribution of low-temperature products C_7KET and C_8KET. As the height increases, CH_2O diffuses to the center of the flame, and the concentration gradually decreases. The range of the distribution area of CH_2O is consistent with the range of the cool flame, *n*-heptane > iso-octane > toluene.

There are two peaks of CH_2O on the central axis of the *n*-heptane and iso-octane flames, as shown in Figure 6. Their lower peaks appear at the same height around an HAB of 8 mm, which are produced by low-temperature reactions. The *n*-heptane flame has more CH_2O radicals, indicating a longer low-to-high temperature reaction in the *n*-heptane flame that causes the CH_2O accumulation. It is seen that the CH_2O radicals decrease dramatically corresponding to the start of second ignition. The second peaks appear at round HABs of 25 and 27 mm, respectively. The CH_2O radicals in this zone are produced through small-molecule reaction $CH_3OCH_2 = CH_2O + CH_3$ and $CH_3O (+M) = CH_2O + H (+M)$, which only happens under high-temperature conditions. The toluene
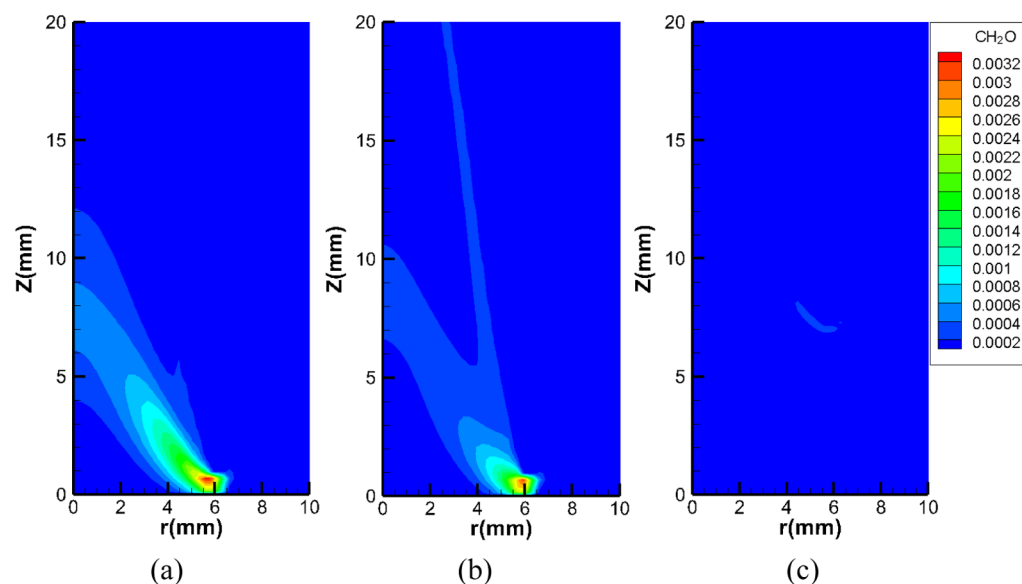

Figure 5. CH_2O distributions of the *n*-heptane, iso-octane, and toluene flames, (a) *n*-heptane, (b) iso-octane, and (c) toluene.
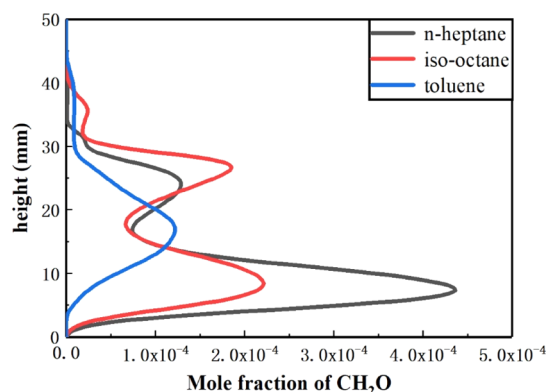
Figure 6. Distributions of CH_2O on the central axis of the *n*-heptane, iso-octane, and toluene flames.

flame has only one CH_2O peak and a lower mole fraction due to the unobtrusive low-temperature reactions.

3.3. PAH Distributions. The two-dimensional distributions of soot volume fraction for three fuels are shown in Figure 7. The soot distribution area and the overall amount of
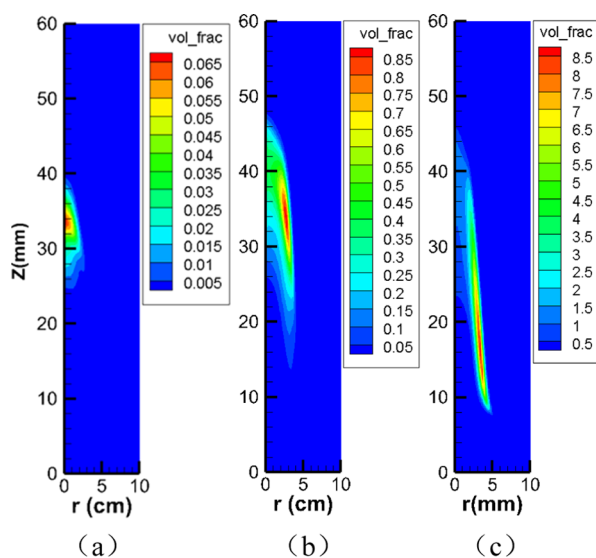

Figure 7. Soot distribution of the *n*-heptane, iso-octane, and toluene flames, (a) *n*-heptane, (b) iso-octane, and (c)toluene.

soot in the toluene flame are the highest. A large amount of soot is generated on the wing of the flame from about an HAB of 8 mm and almost covers the whole flame area. This simulation, to a certain extent, underestimates the soot along the centerline, and the problem exists in other numerical simulations as well.[22,28,40] This deficiency in the soot formation prediction is quite likely caused by the oversimplified assumption that soot nucleation is initiated by the collision of two pyrene (A4) molecules, whereas the soot nucleation process involves multiple PAHs of different sizes in reality. The flame of *n*-heptane, which has the strongest NTC behavior, generates the least soot particles and the smallest soot distribution area. The *n*-heptane flame starts to generate soot particles at around an HAB of 25 mm, and the amount is 2 orders of magnitude less than that of toluene. The amount of soot particles and the distribution area of iso-octane are in between those of the *n*-heptane and toluene flames since the

low-temperature reaction intensity is also in between the other two flames.

The distributions of four aromatic hydrocarbons A1−A4 of *n*-heptane, iso-octane, and toluene flames on the central axis are presented in Figure 8. A1 is considered as the initial precursor of soot formation, and the amount of A4 can indirectly characterize the soot amount. Both *n*-heptane and iso-octane belong to alkane, but the PAH distribution of the two flames is quite different. The quantity of A1−A4 in the iso-octane flame is generally higher than that in the *n*-heptane flame, which is consistent with the soot emission results. Comparing the height of the first peak of A1 and the peak of A2−A4, the higher the number of rings, the higher the position of PAHs, which suggest that A1 evolve to high-ring soot precursors. For the four PAH distributions of the *n*-heptane and iso-octane flames, there are several peaks in the A1 distribution, while A2−A4 are unimodal.

The PAH growth mechanism used in this work follows these rules. All the ring growth reactions are reversible reactions. The collision of two A4 radicals will generate soot particles, and this reaction is irreversible. According to these two rules, when the radical pool concentration of A4 increases to a certain extent, the probability of pairwise molecule collision increases, so more soot is produced. Then, more low-ring PAHs convert to high-ring PAHs to supplement the A4 radical pool. After such a steady stream of transportation, eventually, all converted into soot. However, at some certain stage, where the radical pools of A2 and A3 are abundant, the reactions may change the direction and break down to form A1 to maintain the equilibrium. Therefore, the upper peaks of A1 may be due to the reverse reaction of PAH growth.

The distribution of A1 in the iso-octane flame in the range of HABs of 5−20 mm is quite different from that of *n*-heptane. The amount of A1 in the *n*-heptane flame gradually increases with the increase of the height, reaching its peak at an HAB of 27 mm, and then decreases rapidly, whereas the iso-octane flame reaches its first peak at an HAB of 15 mm with a higher amount. As the flame height can be equivalent to the flame development time, the higher the flame height, the longer time the flame develops. By a comprehensive comparison among the flame height ranges of the keto-peroxide, CH_2O, and A_1, a conversion path from keto-peroxide → CH_2O → A1 can be concluded as each of these radicals peaks at HABs of 6, 8, and 15 mm for the first time. In addition, the A1 formation is seen to be closely related to CH_2O radicals since their distributions on the central axis are quite similar. Toluene is an aromatic hydrocarbon fuel, which hardly reacts under low-temperature conditions. However, it contains a ring structure, which makes it is easy to generate a much larger amount of PAHs, compared with the other alkanes as seen in the figure, under high-temperature conditions. To make it easier to see, the value of A1 in the toluene flame is divided by 50, and the values of A2 and A3 are divided by 20.

Since the mechanism adopted in this work is a reduced mechanism, reactions related to A1 formation shown in Table 2 are the filtrated ones which are of significant importance by sensitivity analysis and rate of production (ROP) analysis. According to these reactions, the formation of A1 is closely related to small molecular hydrocarbons C_2−C_4, which are C_3H_3, C_4H_5, C_2H_2, and C_3H_4. Toluene has a ring structure and generates a large amount of monocyclic aromatic hydrocarbon A1 through the path $C_6H_5CH_3$ (toluene) + H = A1 (benzene) + CH_3. Therefore, the formation of A1 in the toluene flame is
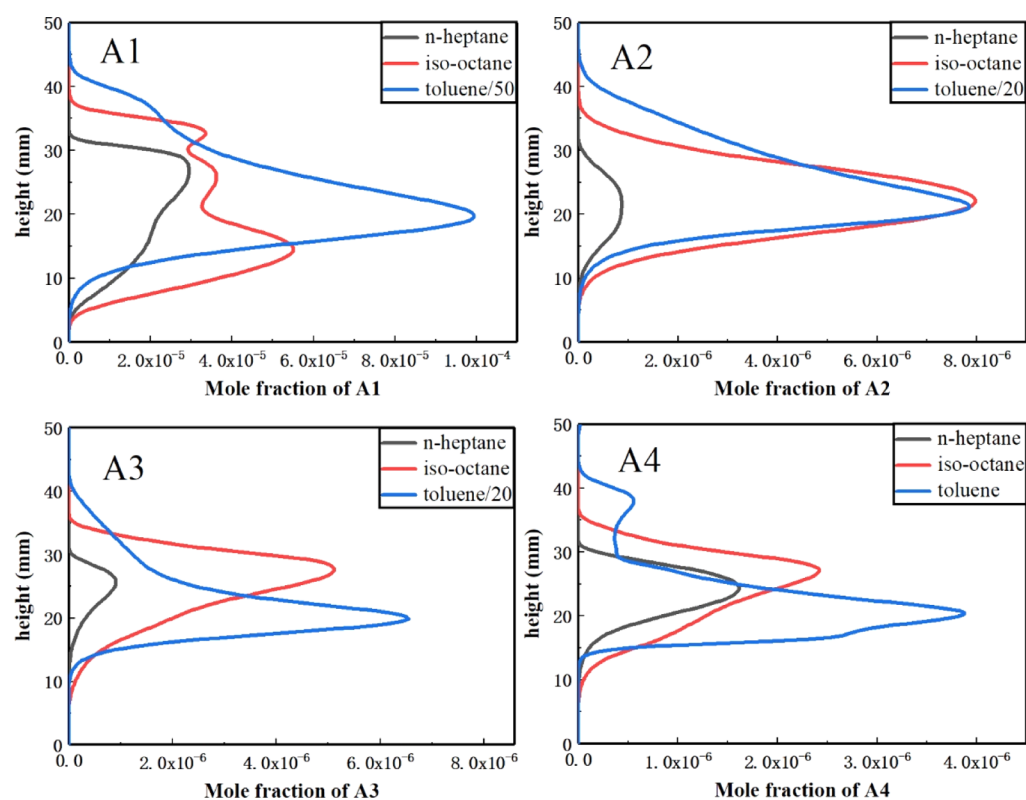
Figure 8. Distributions of A1−A4 on the central axis of the *n*-heptane, iso-octane, and toluene flames.

Table 2. Reactions about the Generation of A1 in the Adoped Mechanism

R33	$C_6H_5CH_3 + H = A1 + CH_3$
R198	$2C_3H_3 = A1$
R199	$C_3H_4 + C_3H_3 = A1 + H$
R200	$C_4H_5 + C_2H_2 = A1 + H$

less affected by small molecular hydrocarbons above. The respective distributions of these small molecular hydrocarbons on the central axis in the three flames are shown in Figure 9. The distributions of C_3H_3 in the three flames are compared in Figure 9a. For the alkanes, the C_3H_3 radicals show a two-hump trend, which start from an HAB of 10 mm and rapidly increase around an HAB of 20. This infers that the C_3H_3 radicals correspond to the A1 accumulations in the alkane fuels at around an HAB of 25 mm through the reaction R198, $C_3H_3 + C_3H_3 = A1$ but have little relationship with the A1 accumulation of the iso-octane flame at an HAB of 15 mm. In comparison, the amount of C_3H_3 in the toluene flame is large, but it is mainly distributed in the zone of HABs of 20−40 mm, even higher than the aggregation position of A1−A4. Therefore, it is inferred that the main source of A1 in toluene flames is not C_3H_3 but directly generated from toluene. The large amount of C_3H_3 comes from the reverse reaction of R198.

As is shown in Figure 9b, the mole fractions of C_4H_5 in the alkane flames occur mainly in the lower zone of flames with a pretty lower order of magnitude of 10^{-8} compared to the other three radicals, while that of the toluene flame is even less. Although C_4H_5 produces A1 through R200, $C_4H_5 + C_2H_2 = A1 + H$, it is not the most important radical in the formation of soot. Figure 9c shows the comparison of C_2H_2 distribution. C_2H_2 is not only the source of A1 formation but also an

important reactant for the conversion of A1 to higher-ring soot precursors in HACA theory. Since the amount of C_4H_5 radicals is low, the portion of C_2H_2 involved in the A1 formation is pretty small according to reaction R200. Most of the C_2H_2 radicals take part in the conversion from A1 to higher-ring soot precursors. The C_2H_2 in the iso-octane flame is generally higher than that in the *n*-heptane flame, which corresponds to the higher soot content of the iso-octane flame. For the toluene flame, the C_2H_2 amount is comparatively low for it is harder to produce C_2H_2 dissociation reactions; however, the large amount of aromatic hydrocarbons still promotes the soot formation rate.

The C_3H_4 distributions are shown in Figure 9d. It is seen that C_3H_4 radicals are about the same magnitude with C_3H_3 but emerge earlier, so the C_3H_4 radicals are a major source of C_3H_3. Compared to the even-carbon small molecules, the odd-carbon small molecules dominate the production of PAHs. It explains the reason that distribution of the iso-octane flame has two peaks on the central axis, while *n*-heptane has only one peak, which is similar to the A1 distribution. Comparing the distribution of these small radicals, it can be found that in the alkane flame, the low-temperature reactions reduce the amount of C_3H_4 produced in the low-temperature region by generating a large amount of CH_2O, which makes A1 to lack reactants in the early reaction, leading to a reduction in soot emissions. In the toluene flame, the small molecular hydrocarbons $C_2−C_4$ have little influence to the formation of A1. However, the lack of C_2H_2 limits the process of aromatic hydrocarbon growth.

3.4. Chemical Analysis of the Low-Temperature Effect. To verify the universality of the above conclusions and understand the phenomenon in the perspective of chemical kinetics, a constant-pressure homogeneous reactor in CHEMKIN software is used to analyze the above three fuel
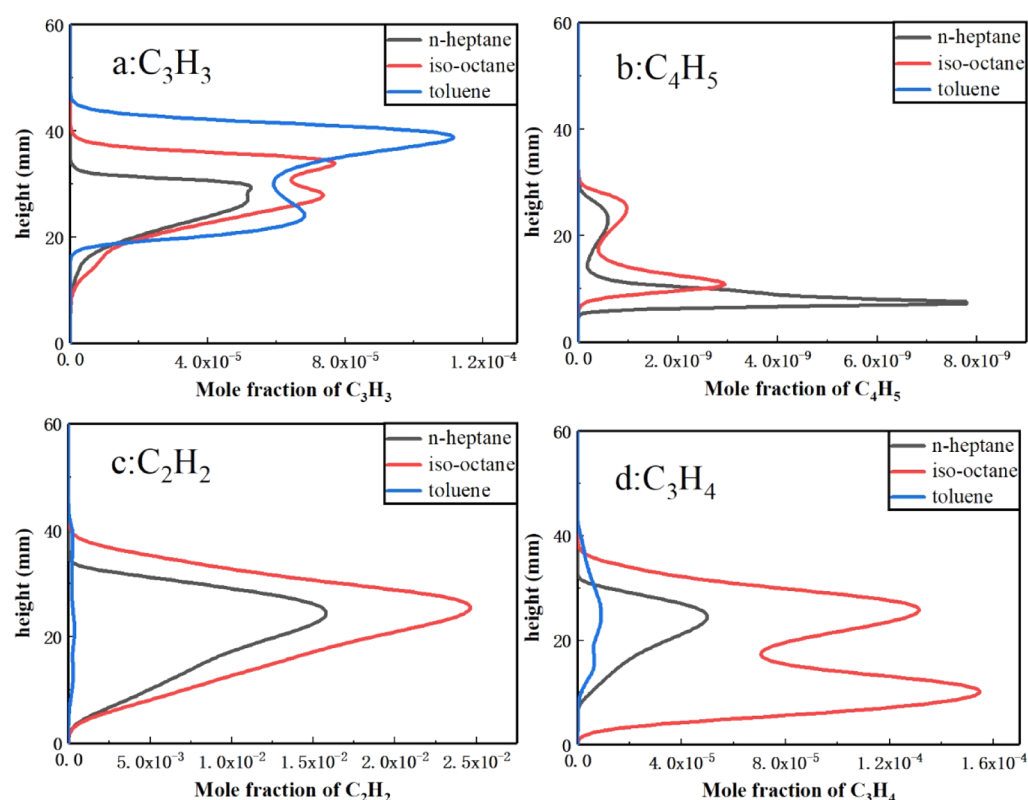
Figure 9. Distributions of C_2-C_4 radicals on the central axis of the *n*-heptane and iso-octane flames.

flames. The ignition delay analysis is conducted for the three fuels, and the results are shown in Figure 10. The ignition
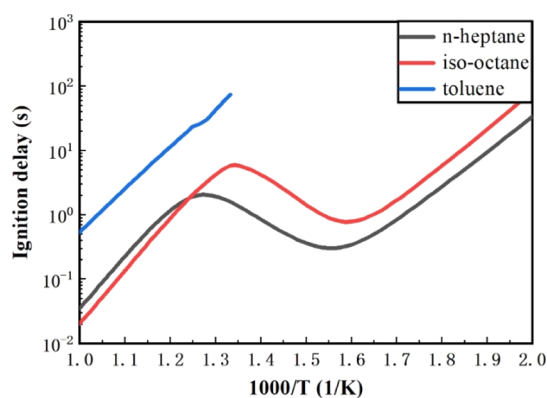

Figure 10. Ignition delays of *n*-heptane, iso-octane, and toluene flames.

formation, a group of simulations with the initial reaction temperature at 700 K are carried out. Figure 11 shows the
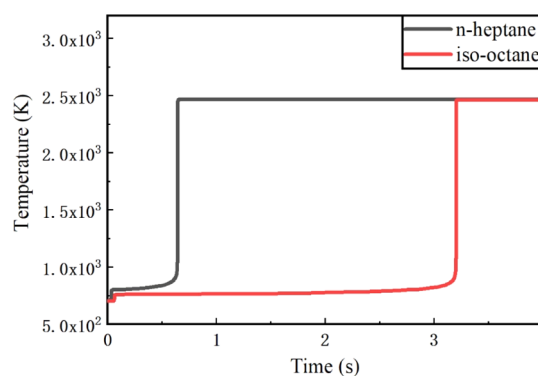

Figure 11. Temperature evolution processes in the flames of *n*-heptane and iso-octane.

delay of toluene is much longer than that of *n*-heptane and iso-octane. In addition, both *n*-heptane and iso-octane have NTC effects and low-temperature reactions. In the *n*-heptane flame, there is a significant NTC trend between $1000/T = 1.28$ and 1.56, while the NTC trend in the iso-octane flame is between $1000/T = 1.34$ and 1.6. Since toluene hardly reacts with air oxidants under low-temperature conditions and little NTC behavior is found, due to its distinct physical and chemical properties and reaction path from those of alkanes, the following text will only focus on the low-temperature reaction in the *n*-heptane and iso-octane flames.

In order to analyze the impact of the chemical mechanism under the low-temperature combustion stage on the soot

temperature changes of *n*-heptane and iso-octane during the reaction. It is seen that both fuels have a two-stage combustion phenomenon, where the first stage of combustion is caused by low-temperature reactions at the beginning. Then, the two fuels enter their second-stage combustion at 0.6 and 3.2 s, respectively.

Figure 12 shows the main reactions associated to the formation of aromatic hydrocarbons A1 at the first-stage combustion in the *n*-heptane flame and the iso-octane flame. For the *n*-heptane flame, C_7H_{16} first undergoes dehydrogenation reaction to produce C_7H_{15}, and then, C_7H_{15} mainly reacts further through three main reaction paths. These three reactions all react under 1000 K, and all contribute to the first-stage combustion. The first path is the oxygen addition
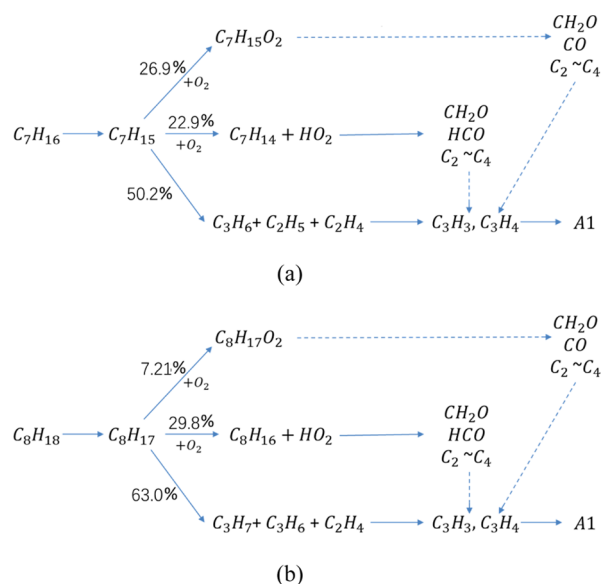
(a)

(b)

Figure 12. Main reaction pathways to aromatic hydrocarbons A_1 of *n*-heptane and iso-octane flames in the first combustion stage. (a) Reaction pathways of *n*-heptane under low-temperature conditions. (b) Reaction pathways of *n*-heptane under low-temperature conditions.

reaction $C_7H_{15} + O_2 = C_7H_{15}O_2$. This reaction accumulates heat and heats up the system, and the subsequent products are CH_2O, CO, and small molecular hydrocarbons. The second reaction path is a chain branching reaction $C_7H_{15} + O_2 = C_7H_{14} + HO_2$. C_7H_{14} reacts with O_2 to generate CH_2O, HCO, and small molecular hydrocarbons; this chain branching reaction slows down the reaction rate and elongates the second-stage ignition, and the NTC behavior appears. The third path is that C_7H_{15} is directly decomposed into C_3H_6, C_2H_5, and C_2H_4, which implies that the system is under a relatively higher temperature than the previous two.

Although the reaction path distribution of iso-octane is similar to that of *n*-heptane, the proportions of the three paths affect the subsequent products. According to the proportion of each reaction path, 26.9% of C_7H_{16} transforms to A_1 through the first reaction path and 22.9% of C_7H_{16} transforms to A_1 through the second path. In total, the percentage for C_7H_{16}

which transforms to A_1 through the first two paths, which produce relatively large molecules, is 49.8%, while only 37% C_8H_{18} transforms to A_1 through the two large-molecule reaction pathways. It can be reasonably inferred that more fuel burned through large-molecule reaction pathways, whose conversion rate is lower, will definitely result in a reduced soot formation. When the fuel burns near the NTC temperature, the flame can be suppressed by NTC to transit to high-temperature flame combustion and stay in the low-temperature zone.

The ROP of the three reaction paths of C_7H_{15} in the *n*-heptane flame and that of C_8H_{17} in the iso-octane flame are compared in Figure 13 to evaluate the intensities of the low-temperature reactions, which affect the ignition delay of both the first- and second-stage combustion. The intensity of the low-temperature reaction $C_7H_{15} + O_2 = C_7H_{15}O_2$ in the *n*-heptane flame is higher than that of the low-temperature reaction $C_8H_{17} + O_2 = C_8H_{17}O_2$ in the isooctane flame. These two oxygen addition reactions generate large molecular radicals and slow down the heat release speed, thus intensifying the NTC effect. Small molecular hydrocarbons such as C_3H_3 and C_2H_2 are also the main sources of aromatic hydrocarbons, while the distribution trend of C_3H_4 is the same as that in the two-dimensional simulation.

Figure 14 shows the mole fractions of key small radicals and A1 during the first-stage combustion of *n*-heptane and iso-octane flames. It is seen that the *n*-heptane flame with stronger low-temperature reaction and weak decomposition reaction will not significantly increase the amount of small molecular hydrocarbons as shown in Figure 14a, compared to the iso-octane flame with weaker low-temperature reaction and strong decomposition reaction, which generates a large amount of C_3H_4 in the first-stage combustion, as shown in Figure 14b. The mole fraction of A1 in the iso-octane flame is greater than that in the *n*-heptane flame. Therefore, the reason that the low-temperature reaction suppresses soot formation is that it inhibits the direct decomposition of large alkyl groups to small molecular hydrocarbons, which promote the PAH formation and the subsequent soot generation process. Figure 15 presents the reaction pathway.

3.5. Comparison of Factors Influencing the Soot Forming Characteristics. The above argument proves that low-temperature reaction can reduce soot emissions in the
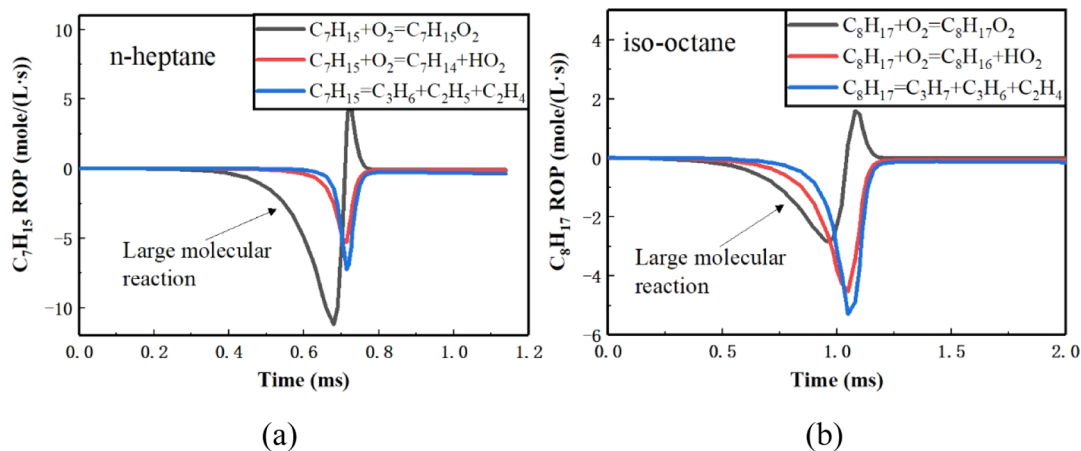

(a)

(b)

Figure 13. Production rates of key branch reactions of C_7H_{15} and C_8H_{17} during the first-stage combustion of *n*-heptane flame and iso-octane flames, (a) *n*-heptane and (b) iso-octane.
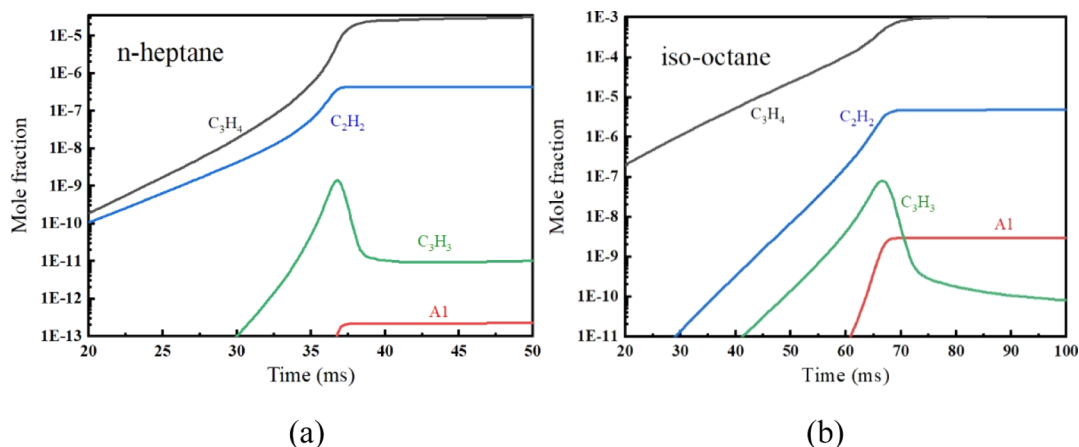
Figure 14. Mole fractions of key small radicals and A1 during the first-stage combustion of *n*-heptane and iso-octane flames, (a) *n*-heptane and (b) iso-octane.
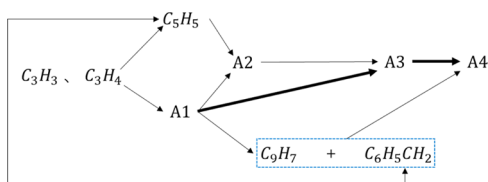

Figure 15. Main reaction pathways of A1−A4 in the alkanes.

Figure 16. Mole fractions of A_1 under different test conditions.

perspective of chemical kinetics, which also confirms that under the laboratory conditions, diesel with stronger NTC behavior releases less soot than gasoline. However, since traditional gasoline engines mostly work in the oil−gas premix combustion mode due to its high volatility, the combustion mixture is relatively uniform, which makes the traditional gasoline engine a cleaner engine than diesel in terms of soot emission. In comparison, the spray combustion mode forms a highly heterogeneous concentration field in the practical diesel engines. Besides, the soot formation in an actual engine is also affected by the cylinder pressure. Therefore, a numerical comparison is conducted in this part to shed light on the weight of low-temperature effects on the soot forming characteristics when compared with other factors.

Therefore, four sets of simulations with different working conditions are conducted. They are stoichiometric *n*-heptane flames with different initial pressures, C_7H_{16}−30 atm−Φ1.0 and C_7H_{16}−60 atm−Φ1.0, rich *n*-heptane flame C_7H_{16}−60 atm−Φ3.0, and stoichiometric iso-octane flame C_8H_{18}−30 atm−Φ1.0, where Φ represents the equivalence ratio. Their relationships of the mole fraction of A1 versus the initial temperature are shown in Figure 16. The mole fraction of A1 of C_7H_{16}−60 atm−Φ1.0 is slightly higher than that of the C_7H_{16}−30 atm−Φ1.0 case when the initial temperature is blow 1050 K, which is generally under the low-temperature conditions, while the mole fraction of A1 of C_7H_{16}−60 atm−Φ1.0 drops slightly down below that of C_7H_{16}−30 atm−Φ1.0 in the high-temperature region. Comparing the results between C_7H_{16}−30 atm−Φ1.0 and C_8H_{18}−30 atm−Φ1.0 with the same reaction pressure and equivalence ratio, *n*-heptane with intensified low-temperature reaction and stronger NTC behavior produces less amount of A1. At last, the results of the *n*-heptane flame under C_7H_{16}−60 atm−Φ3.0 and C_7H_{16}−60 atm−Φ1.0 working conditions with the same reaction pressure but different equivalence ratios show that the

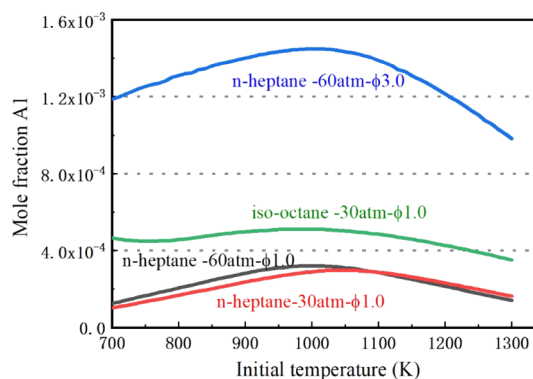rich mixture C_7H_{16}−60 atm−Φ3.0 generates a dramatically large amount of A1 particles, which is an order of magnitude higher than that produced in the stoichiometric flame. The aforementioned comparisons indicate that the equivalence ratio among the three factors has the greatest influence on soot emissions, whereas the low-temperature effect is more important than pressure.

Furthermore, as shown in Figure 17, the ROP of C_7H_{15} at stoichiometric and rich flames varies greatly. The low-temperature reaction $C_7H_{15} + O_2 = C_7H_{15}O_2$ and $C_7H_{15} + O_2 = C_7H_{14} + HO_2$ at the stoichiometric flame takes up a much larger portion than that in the rich flame Φ3.0. The result implies that the suppress effects of low-temperature reaction and NTC on the soot formation are more prominent under lean and stoichiometric conditions. The reason is that due to the lack of oxygen, the combustion in the fuel-rich zone trends to shift toward a decomposition reaction, which requires less oxygen participation. The proportion of high-temperature reaction $C_7H_{15} \geq C_3H_6 + C_2H_5 + C_2H_4$ increases. The amount of small molecular hydrocarbons soars up and promotes soot generation. Therefore, even though diesel has a stronger low-temperature reaction that may improve the soot emission, this effect is not as prominent as that of equivalence ratio and this merit can be degraded largely under fuel-rich conditions.

4. CONCLUSIONS

By numerically simulating the 2-D distributions of the temperature field, soot precursors A1−A4, and the low-temperature reaction in the *n*-heptane, iso-octane, and toluene
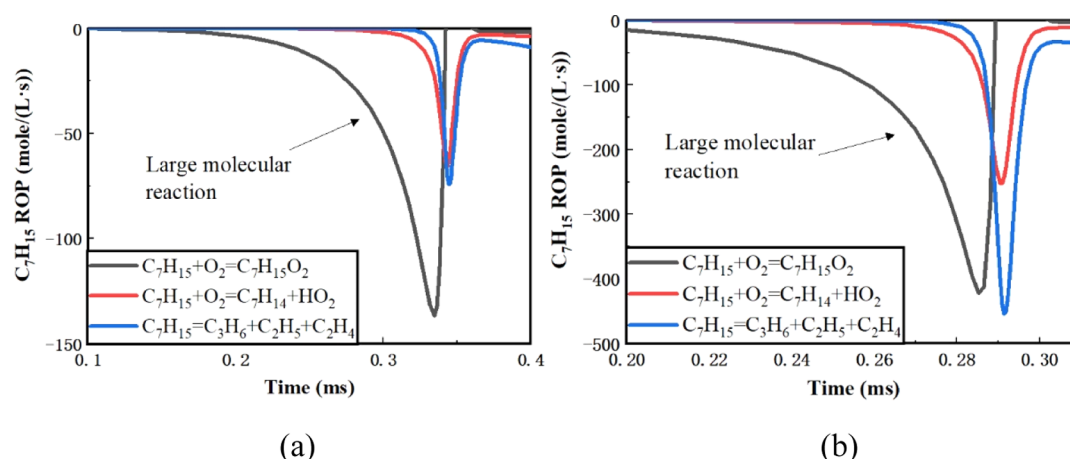
Figure 17. Production rates of three key branch reactions of C_7H_{15} in the *n*-heptane flames at equivalence ratio = 1.0 and 3.0, (a) Φ1.0 and (b) Φ3.0.

flames, the effect of NTC on the formation of soot precursor PAHs, especially the monocyclic-ring benzene (A1), is investigated. Through the comparison with another to physical factors, pressure and equivalence ratio, the weight of NTC and the low-temperature effect are evaluated. The main conclusions are as follows:

(1) The laminar diffusion flame of *n*-heptane, which has a stronger NTC behavior than the iso-octane flame and toluene flame, generates the least soot particles, and the soot distribution area is the smallest among the three.

(2) The keto-peroxide and CH_2O can be considered as the indicators of NTC behavior. The mole fractions of these radicals are less in the iso-octane flame in the "soot-free zone" and are pieces of evidence of weaker NTC effects of iso-octane.

(3) The low-temperature reactions suppress the formation of PAHs by taking the oxygen addition reaction $C_7H_{15} + O_2 = C_7H_{15}O_2$ and $C_7H_{15} + O_2 = C_7H_{14} + HO_2$ to produce large molecular hydrocarbons instead of the disassociation reactions that produce small molecular hydrocarbons, such as C_2H_2, C_3H_3, C_3H_4, and so forth.

(4) In the first combustion stage, 49.8% of C_7H_{16} reacts through the two large molecular reaction pathways, which suppresses the formation of A_1. However, only 37% of C_8H_{18} reacts through large molecular reaction pathways. The more the portion of the fuel burnt through the two large molecular reaction pathways, the less the soot formed in total.

(5) Toluene generates a large amount of monocyclic aromatic hydrocarbon A1 through the path $C_6H_5CH_3 + H = A1 + CH_3$. Therefore, the formation of A1 in the toluene flame is less affected by small molecular hydrocarbons.

(6) The influence of equivalence ratio on soot emissions is much higher than the pressure and NTC effects, and the suppress effects of low-temperature reaction and NTC on the soot formation are more prominent under lean and stoichiometric conditions.

■ AUTHOR INFORMATION

Corresponding Author

Saifei Zhang − *School of Mechanical Engineering, Beijing Institute of Technology, Beijing 100081, China;* orcid.org/ 0000-0002-6254-2695; Phone: +86-10-68918581; Email: saifeizhang@hotmail.com

Authors

Han Wu − *School of Mechanical Engineering, Beijing Institute of Technology, Beijing 100081, China;* orcid.org/0000-0002-9113-9774

Zhen Hu − *School of Mechanical Engineering, Beijing Institute of Technology, Beijing 100081, China*

Xu Dong − *Shandong Shuanggang Piston Co., Ltd., Rizhao 276800, Shandong, China*

Zhikun Cao − *School of Mechanical Engineering, Beijing Institute of Technology, Beijing 100081, China*

Sheng-lun Lin − *School of Mechanical Engineering, Beijing Institute of Technology, Beijing 100081, China;* orcid.org/ 0000-0003-2035-7456

Complete contact information is available at:
https://pubs.acs.org/10.1021/acsomega.1c01397

Notes
The authors declare no competing financial interest.

■ ACKNOWLEDGMENTS

■ REFERENCES

(1) Inal, F.; Senkan, S. M. Effects of oxygenate additives on polycyclic aromatic hydrocarbons (PAHs) and soot formation. *Combust. Sci. Technol.* **2002**, *174*, 1−19.

(2) Guerrero Peña, G. D. J.; Hammid, Y. A.; Raj, A.; Stephen, S.; Anjana, T.; Balasubramanian, V. On the characteristics and reactivity of soot particles from ethanol-gasoline and 2,5-dimethylfuran-gasoline blends. *Fuel* **2018**, *222*, 42−55.

(3) Shi, Z.; Wu, H.; Li, H.; Zhang, L.; Li, X.; Lee, C.-f. Effect of injection pressure and fuel mass on wall-impinging ignition and combustion characteristics of heavy-duty diesel engine at low temperatures. *Fuel* **2021**, *299*, 120904.

(4) Liu, Y.; Gao, Y.; Yu, N.; Zhang, C.; Wang, S.; Ma, L.; Zhao, J.; Lohmann, R. Particulate matter, gaseous and particulate polycyclic aromatic hydrocarbons (PAHs) in an urban traffic tunnel of china: emission from on-road vehicles and gas-particle partitioning. *Chemosphere* **2015**, *134*, 52−59.

(5) Maurice, L. Q.; Lander, H.; Edwards, T.; Harrison, W. E., III Advanced aviation fuels: a look ahead via a historical perspective. *Fuel* **2001**, *80*, 747−756.

(6) Saffaripour, M.; Chan, T. W.; Liu, F.; Thomson, K. A.; Smallwood, G. J.; Kubsh, J.; Brezny, R. Effect of Drive Cycle and Gasoline Particulate Filter on the Size and Morphology of Soot Particles Emitted from a Gasoline-Direct-Injection Vehicle. *Environ. Sci. Technol.* **2015**, *49*, 11950−11958.

(7) Lapuerta, M.; Rodríguez−Fernández, J.; Sánchez-Valdepeñas, J. Soot reactivity analysis and implications on diesel filter regeneration. *Prog. Energy Combust. Sci.* **2020**, *78*, 100833.

(8) Yamamoto, K.; Toda, Y. Numerical Study on Filtration of Soot Particulates in Gasoline Exhaust Gas by SiC Fiber Filter. *Key Eng. Mater.* **2017**, *735*, 119−124.

(9) An, Y.-z.; Pei, Y.-q.; Qin, J.; Zhao, H.; Teng, S.-p.; Li, B.; Li, X. Development of a PAH (polycyclic aromatic hydrocarbon) formation model for gasoline surrogates and its application for GDI (gasoline direct injection) engine CFD (computational fluid dynamics) simulation. *Energy* **2016**, *94*, 367−379.

(10) Zheng, L.; Ma, X.; Wang, Z.; Wang, J. An optical study on liquid-phase penetration, flame lift-off location and soot volume fraction distribution of gasoline-diesel blends in a constant volume vessel. *Fuel* **2015**, *139*, 365−373.

(11) An, Y.-z.; Teng, S.-p.; Pei, Y.-q.; Qin, J.; Li, X.; Zhao, H. An experimental study of polycyclic aromatic hydrocarbons and soot emissions from a GDI engine fueled with commercial gasoline. *Fuel* **2016**, *164*, 160−171.

(12) Liu, F.; Gao, Y.; Wu, H.; Zhang, Z.; He, X.; Li, X. Investigation on Soot Characteristics of Gasoline/Diesel Blends in a Laminar Coflow Diffusion Flame. *Energy Fuels* **2018**, *32*, 7841−7850.

(13) Kholghy, M. R.; Weingarten, J.; Sediako, A. D.; Barba, J.; Lapuerta, M.; Thomson, M. J. Structural effects of biodiesel on soot formation in a laminar coflow diffusion flame. *Proc. Combust. Inst.* **2016**, *36*, 1321−1328.

(14) Liu, F.; Hua, Y.; Wu, H.; Lee, C.-f.; Li, Y. Experimental Investigation of Polycyclic Aromatic Hydrocarbons Growth Characteristics of Gasoline Mixed with Methanol, Ethanol, or n-Butanol in Laminar Diffusion Flames. *Energy Fuels* **2018**, *32*, 6823−6833.

(15) Liu, F.; Hua, Y.; Wu, H.; Lee, C.-f. Effect of Toluene Addition on the PAH Formation in Laminar Coflow Diffusion Flames of n-Heptane and Isooctane. *Energy Fuels* **2018**, *32*, 7142−7152.

(16) Saffaripour, M.; Veshkini, A.; Kholghy, M.; Thomson, M. J. Experimental investigation and detailed modeling of soot aggregate formation and size distribution in laminar coflow diffusion flames of Jet A-1, a synthetic kerosene, and n-decane. *Combust. Flame* **2014**, *161*, 848−863.

(17) Zhang, Y.; Liu, F.; Clavel, D.; Smallwood, G. J.; Lou, C. Measurement of soot volume fraction and primary particle diameter in oxygen enriched ethylene diffusion flames using the laser-induced incandescence technique. *Energy* **2019**, *177*, 421−432.

(18) Stadler, D.; Rossi, M. J. The reactivity of no2 and hono on flame soot at ambient temperature: the influence of combustion conditions. *Phys. Chem. Chem. Phys.* **2000**, *2*, 5420−5429.

(19) Payri, R.; Gimeno, J.; Cardona, S.; Ayyapureddi, S. Experimental study of the influence of the fuel and boundary conditions over the soot formation in multi-hole diesel injectors using high-speed color diffused back-illumination technique. *Appl. Therm. Eng.* **2019**, *158*, 113746.

(20) Hayashida, K.; Mogi, T.; Amagai, K.; Arai, M. Growth characteristics of polycyclic aromatic hydrocarbons in dimethyl ether diffusion flame. *Fuel* **2011**, *90*, 493−498.

(21) Lee, S. M.; Yoon, S. S.; Chung, S. H. Synergistic effect on soot formation in counterflow diffusion flames of ethylene-propane mixtures with benzene addition. *Combust. Flame* **2004**, *136*, 493−500.

(22) Liu, F.; He, X.; Ma, X.; Zhang, Q.; Thomson, M. J.; Guo, H.; Smallwood, G. J.; Shuai, S.; Wang, J. An experimental and numerical study of the effects of dimethyl ether addition to fuel on polycyclic aromatic hydrocarbon and soot formation in laminar coflow ethylene/air diffusion flames. *Combust. Flame* **2011**, *158*, 547−563.

(23) Liu, F.; Hua, Y.; Wu, H.; Lee, C. f.; Shi, Z. Experimental and kinetic studies of soot formation in methanol-gasoline coflow diffusion flames. *J. Energy Inst.* **2019**, *92*, 38−50.

(24) Liu, F.; Hua, Y.; Wu, H.; Lee, C.-f.; He, X. An experimental study on soot distribution characteristics of ethanol-gasoline blends in laminar diffusion flames. *J. Energy Inst.* **2018**, *91*, 997−1008.

(25) Li, Y.; Zhang, Y.; Zhan, R.; Huang, Z.; Lin, H. Study of pah formation in laminar premixed toluene and c8h10 aromatics flames. *Fuel* **2020**, *275*, 117774.

(26) Chu, C.; Thomson, M. J. The effects of naphthalene-addition to alkylbenzenes on soot formation. *Combust. Flame* **2020**, *215*, 169−183.

(27) Chu, H.; Ya, Y.; Nie, X.; Qiao, F.; Jiaqiang, E. Effects of adding cyclohexane, n-hexane, ethanol, and 2,5-dimethylfuran to fuel on soot formation in laminar coflow n-heptane/iso-octane diffusion flame. *Combust. Flame* **2021**, *225*, 120−135.

(28) Consalvi, J.-L.; Liu, F.; Kashif, M.; Legros, G. Numerical study of soot formation in laminar coflow methane/air diffusion flames doped by n- heptane/toluene and iso-octane/toluene blends. *Combust. Flame* **2017**, *180*, 167−174.

(29) Hansen, N.; Cool, T. A.; Westmoreland, P. R.; Kohse-Höinghaus, K. Recent contributions of flame-sampling molecular-beam mass spectrometry to a fundamental understanding of combustion chemistry. *Prog. Energy Combust. Sci.* **2009**, *35*, 168−191.

(30) Appel, J.; Bockhorn, H.; Frenklach, M. Kinetic modeling of soot formation with detailed chemistry and physics: laminar premixed flames of C2 hydrocarbons. *Combust. Flame* **2000**, *121*, 122−136.

(31) Marchal, C.; Delfau, J.-L.; Vovelle, C.; Moréac, G.; Mounaïm-Rousselle, C.; Mauss, F. Modelling of aromatics and soot formation from large fuel molecules. *Proc. Combust. Inst.* **2009**, *32*, 753−759.

(32) Ciajolo, A.; Alfe, M.; Apicella, B.; Barbella, R.; Tregrossi, A. Characterization of carbon particulate matter relevant in combustion. *9th International Conference on Chemical and Process Engineering* 2009, Vol. *17*, pp 99−104.

(33) Wang, H.; Jiao, Q.; Yao, M.; Yang, B.; Qiu, L.; Reitz, R. D. Development of an n-heptane/toluene/polyaromatic hydrocarbon mechanism and its application for combustion and soot prediction. *Int. J. Engine Res.* **2013**, *14*, 434−451.

(34) Liu, X.; Wang, H.; Wei, L.; Liu, J.; Reitz, R. D.; Yao, M. Development of a reduced toluene reference fuel (TRF)-2,5-dimethylfuran- polycyclic aromatic hydrocarbon (PAH) mechanism for engine applications. *Combust. Flame* **2016**, *165*, 453−465.

(35) Wang, H.; Frenklach, M. A detailed kinetic modeling study of aromatics formation in laminar premixed acetylene and ethylene flames. *Combust. Flame* **1997**, *110*, 173−221.

(36) Zhang, C.; Chen, L.; Ding, S.; Xu, H.; Li, G.; Consalvi, J.-L.; Liu, F. Effects of soot inception and condensation PAH species and fuel preheating on soot formation modeling in laminar coflow CH4/air diffusion flames doped with n-heptane/toluene mixtures. *Fuel* **2019**, *253*, 1371−1377.

(37) Zhao, P.; Law, C. K. The role of global and detailed kinetics in the first-stage ignition delay in NTC-affected phenomena. *Combust. Flame* **2013**, *160*, 2352−2358.

(38) Law, C. K.; Zhao, P. NTC-affected ignition in nonpremixed counterflow. *Combust. Flame* **2012**, *159*, 1044−1054.

(39) Liu, F.; Hua, Y.; Wu, H.; Lee, C.-f.; He, X. Effect of alcohol addition to gasoline on soot distribution characteristics in laminar diffusion flames. *Chem. Eng. Technol.* **2018**, *41*, 897−906.

(40) Cepeda, F.; Jerez, A.; Demarco, R.; Liu, F.; Fuentes, A. Influence of water-vapor in oxidizer stream on the sooting behavior for laminar coflow ethylene diffusion flames. *Combust. Flame* **2019**, *210*, 114−125.